Nanoscale Turing structures

Piotr Dziekan,[1,2,a)] J. S. Hansen,[3] and Bogdan Nowakowski[1,4]
[1]*Institute of Physical Chemistry, Polish Academy of Sciences, Kasprzaka 44/52, 01-224 Warsaw, Poland*
[2]*Laboratoire de Physique Théorique de la Matière Condensée (LPTMC), Université Pierre et Marie Curie – Paris 06, 4 place Jussieu, case courrier 121, 75252 Paris cedex 05, France and CNRS UMR 7600, LPTMC, Paris, France*
[3]*The Department of Science, Systems and Models, Roskilde University, DNRF Centre "Glass and Time," Universitetsvej 1, bygn. 27, DK-4000, Roskilde, Denmark*
[4]*Physics Laboratory, Warsaw University of Life Sciences – SGGW, Nowoursynowska 159, 02-776 Warsaw, Poland*

(Received 18 June 2014; accepted 5 September 2014; published online 23 September 2014)

Formation of Turing patterns of nanoscopic length scale is simulated using molecular dynamics. Based on Fourier spectra of the concentrations of species, we compare stabilities of the structures of different wavelengths and for different intermolecular potentials. Long range attraction is shown to oppose the formation of structures. Our simulations suggest that Turing patterns can be a method of self-organization at a length scale of down to 20 molecular diameters. © *2014 AIP Publishing LLC*. [http://dx.doi.org/10.1063/1.4895907]

I. INTRODUCTION

Alan Turing showed that a spatially uniform stationary state of a nonlinear chemical system can be unstable to nonuniform perturbations if the diffusivities of the reactants are different.[1] This diffusion-driven instability leads to a spontaneous formation of stable structures of the reactant concentrations. The mechanism is believed to be responsible for the formation of numerous types of patterns observed in biology[2] and has also been reproduced in chemical experiments.[3] Wavelengths of Turing patterns considered usually start from the micrometer range. On the other hand, phenomena typical for nonlinear reaction-diffusion systems, like bistability, wave propagation and pattern formation, are observed at the nanoscale in systems with heterogeneous catalysis.[4–7] These phenomena were analyzed theoretically using kinetic and master equations.[8,9] In addition, reaction-diffusion systems were used to fabricate nanoscopic materials by imposing specific initial conditions.[10]

Our goal is to see if nanoscopic patterns can spontaneously form through the Turing mechanism. To this end, we present for the first time molecular dynamics (MD) simulations of Turing patterns. We already performed simulations of Turing patterns at the mesoscopic level[11] and at the microscopic level in rarefied media.[12] The MD method is suitable for dense media, and closely models real system dynamics. MD is useful in both explaining experimental results and as a reference for other methods. MD simulations intrinsically include internal fluctuations, do not rely on macroscopic parameters, like diffusivities, and capture the non-Markovian nature of collisions, as well as long range correlations. Use of other methods, like the master or kinetic equations, which require additional approximations, has to be justified by comparison with microscopic simulations, if no experimental results are available.

Using MD simulations we show that, despite fluctuations, Turing patterns can develop with as little as 20 particles per wavelength. Therefore, the Turing mechanism can be regarded as a method of self-organization of molecules at the nanoscale. It is not an equilibrium phase separation resulting from intermolecular interactions, but a consequence of system dynamics and can be seen only if the system is far from equilibrium. If one would like to manufacture a nanostructured material, the method would require an additional step, e.g., photopolymerization, that would bind molecules and preserve positional inhomogeneity of the dissipative structure. An advantage of this method is that the Turing mechanism is known to produce many different types of structures, so a variety of shapes could be obtained by changing reaction conditions. Furthermore, we show that although formation of Turing patterns requires a specific type of reactions between two species, using one pair of such reactants it would be possible to generate structures of other particle types.

II. MODEL

We use a simple reaction scheme in which Turing patterns can be observed:

$$\mathrm{A} \xrightarrow{k_1} \mathrm{R}_1, \tag{1}$$

$$2\mathrm{A} + \mathrm{B} \xrightarrow{k_2} 3\mathrm{A}, \tag{2}$$

$$\mathrm{B} \underset{k'_{-3}}{\overset{k_3}{\rightleftharpoons}} \mathrm{R}_2. \tag{3}$$

R_2 is a substrate and R_1 a product of the reaction. Their concentrations are kept constant by appropriate feeding and

a)Author to whom correspondence should be addressed. Electronic mail: pdziekan@ichf.edu.pl. Tel.: +48 22 343 3314.

removal, which keeps the system out of equilibrium. Macroscopically, the model is equivalent to the Gray–Scott model, as the equations governing evolution of concentrations are the same in both cases and have the form[13]

$$\partial_t A(\boldsymbol{r},t) = k_2 A(\boldsymbol{r},t)^2 B(\boldsymbol{r},t) - k_1 A(\boldsymbol{r},t) + D_A \Delta A(\boldsymbol{r},t), \tag{4}$$

$$\partial_t B(\boldsymbol{r},t) = -k_2 A(\boldsymbol{r},t)^2 B(\boldsymbol{r},t) - k_3 B(\boldsymbol{r},t) + k_{-3} + D_B \Delta B(\boldsymbol{r},t), \tag{5}$$

where $k_{-3} = k'_{-3} R_2$, D_A and D_B are the diffusion coefficients and Δ is the Laplacian.

In case of a homogeneous system, there may be three stationary states: $(A_0 = 0, B_0)$, (A_-, B_-), and (A_+, B_+). The latter two states can be obtained by solving the equation

$$A^2 - \frac{k_{-3}}{k_1} A + \frac{k_3}{k_2} = 0 \tag{6}$$

and using $B = \frac{k_1}{k_2 A}$.

The state $(A_0 = 0, B_0)$ is always a stable node and the state (A_-, B_-) is a saddle point. The third state (A_+, B_+) can be either stable or unstable and it is the state from which Turing pattern can develop. Linear stability analysis towards spatially harmonic perturbations shows that, if diffusion coefficients of A and B are sufficiently different, there can be a range of growing modes. The smallest λ_{min} and largest λ_{max} possible wavelengths of the spatial structure can be calculated, as well as the fastest growing wavelength λ_0, where $\lambda_{min} < \lambda_0 < \lambda_{max}$. In finite systems, boundary conditions restrict the allowed modes. In the long time limit the allowed mode with highest growth rate should dominate, but in some cases a transient structure of different wavelength is seen.[12]

III. SIMULATION METHOD

The major difficulty in simulating Turing structures using MD lies in obtaining sufficiently different diffusion coefficients for A and B. In our previous paper,[12] we described a method to simulate Turing patterns in rarefied media. Particles were assumed to have different sizes, which results in different mobilities. However, in dense media this simple mechanism of abrupt change of size cannot be used as it would lead to particles overlapping. Therefore, in the MD simulations we limit mobility of one species by binding it to a third type of particle, which is heavy, nonreactive, and labeled H. This way of imposing different diffusivities is inspired by the chlorite-iodide-malonic acid (CIMA) reaction, where inhibitor molecules bind to micelles.[14] To analyse effects of intermolecular attraction we perform simulations for both the Lennard-Jones (LJ) and Weeks-Chandler-Andersen (WCA) potentials.[15,16]

There are four types of particles in the system: A, B, R, and H. The R species act as both the R_1 and R_2 species in the reaction scheme. All particles have same sizes. The reactive A, B, and R particles also have the same, unit masses. We use the usual reduced MD units.[17] Type H particles are much heavier (their mass is denoted by m_H, in most cases we use $m_H = 10^4$) and do not take part in the reaction scheme, but are able to bind type A molecules. The bond between A and H is formed whenever the distance between particles is in the range $r_b \pm 0.01$, where $r_b = 0.95$ is the bond length. The bond is broken if the particles become separated by more than 1.25. At one time, a single bond between A and H particles can be formed. Whenever reaction turns a bonded A into a B, the bond is broken. Formation and breaking of bonds this way does not conserve energy. Therefore, temperature is controlled by a Nose–Hoover thermostat at $T = 2.65$, the Boltzmann constant is set to 1 and simulation time step to $\Delta t = 2.1 \times 10^{-3}$. The bound particles interact with an additional Gaussian potential well

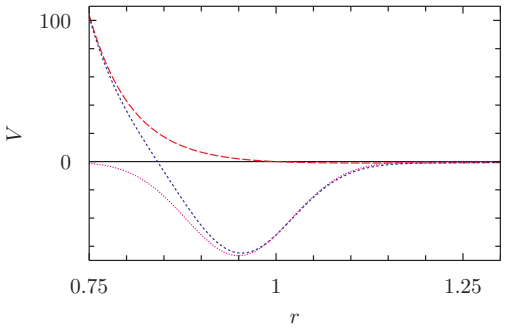

FIG. 1. Intermolecular potentials used. The dashed line is the standard Lennard-Jones potential, with $\sigma = 1$ and $\epsilon = 1$. The solid line is the bond potential with parameters $\sigma_b^2 = 0.5$, $\epsilon_b = 66.67$, and $r_b = 0.95$. The dotted line is a sum of both potentials.

$$V_{bond}(r) = -\epsilon_b \exp\left[-\frac{(r - r_b)^2}{2\sigma_b^2}\right]. \tag{7}$$

The pair potentials are shown in Fig. 1.

Initially, all particles are equally spaced on a cubic arrangement with spacing $\Delta l = \rho^{-1/3}$, where $\rho = 0.7$ is the density. This density corresponds to a supercritical LJ fluid. Number of particles in each direction is denoted by n_x, n_y, and n_z. Therefore, dimensions of the simulation box are $l_x = n_x \Delta l$, $l_y = n_y \Delta l$, and $l_z = n_z \Delta l$. Since we are interested in simulating 1D patterns, l_z is set to be larger, while l_x and l_y to be smaller than minimal wavelength λ_{min}. We use periodic boundary conditions.

The number of particles to react according to the unimolecular reactions (1) and (3) is sampled from the binomial distribution at each time step. Then, random particles of respective species have their types changed. To simulate a constant concentration of R, rate of reverse reaction (3) is constant and equal to $k_{-3} V$. Moreover, it has to be the same throughout the system, independent of local number of R particles. Therefore, sampling and selection of particles to react is performed independently for each subvolume of length Δl along the z axis.

The trimolecular reactions are performed according to a distance criterion. It occurs whenever the distance of each of the appropriate three molecules from their center of mass is shorter than r_r. This parameter is used to control value of the rate constant k_2.

We expect to observe a spatial structure in concentrations of species A and B. Consequently, we want to simulate as

many particles of these types as possible. However, a couple of constraints have to be considered when setting initial concentrations of the species. First, the number of H particles has to be high, to ensure that every newly created A particle is quickly bonded. Then, population of R particles cannot be too low, because they are needed to perform reverse reaction (3) uniformly throughout the system.

After the system size, initial species concentrations and reaction distance r_r are defined, a preliminary simulation is carried out to estimate the effective diffusion coefficients and the trimolecular reaction rate k_2 for homogeneous system in the initial state. Having these values, we impose that the initial species concentrations correspond to the stationary state (A_+, B_+) of the system of equations (4) and (5). Then, the unimolecular reaction rate k_1 is obtained from Eq. (4):

$$k_1 = k_2 A_+ B_+. \tag{8}$$

From the free term of Eq. (6) follows an expression for k_3:

$$k_3 = k_2 A_+ A_-. \tag{9}$$

This equation includes the position A_- of the saddle point along A axis of phase space, which will be considered as one of the parameters of the model. Then, expression for the last rate constant is readily obtained from Eq. (5):

$$k_{-3} = k_2 A_+^2 B_+ + k_3 B_+. \tag{10}$$

The simulation program was based on the seplib library.[18]

IV. RESULTS

Our first goal was to obtain spatial structures and confirm that they are formed by the Turing mechanism. To this end we performed simulations for parameters deep in the Turing region using the WCA potential. The effect of intermolecular attraction will be discussed later. Turing structure wavelength is defined solely by values of rate constants and diffusivities and is independent of the system dimensions, if one disregards effects of boundary conditions. Therefore, increasing length of the system by two should yield a structure of the same wavelength.

Simulation box size in the directions perpendicular to main axis z was set to $l_x = l_y = 12\Delta l$. The initial concentrations of species were: $A_{init} = A_+ = 0.15\rho$, $B_{init} = B_+ = 0.23\rho$, $R_{init} = 0.12\rho$, $H_{init} = 0.5\rho$, and we fix the saddle point position at $A_- = 1.5 \times 10^{-2}$. The parameter values given above were the same for all simulations presented in this paper. This choice of parameters results in a condition for diffusivities $D_B/D_A > 3.57$ and also implies that the stationary state (A_+, B_+) is an unstable focus. Integration of the deterministic equations (4) and (5) shows that if the diffusivities do not fulfill the condition $D_B/D_A > 3.57$, the system will develop towards homogeneous (A_0, B_0) state, but for diffusivities satisfying it, a periodic structure should emerge.

Moreover, to confirm that the A-H bonds do not impose any spatial structure and to calculate diffusion coefficients at the stationary state we performed simulations with bond formation, but without chemical reactions. The system remained homogeneous and the observed diffusivities of species were $D_A \approx 7.6 \times 10^{-3}$ and $D_B \approx 7.5 \times 10^{-2}$. Then we started simulations with chemical reactions. We set the reaction distance to $r_r = 0.56$, which gives an average trimolecular rate constant $k_2 \approx 7.2 \times 10^{-2}$. That gives possible structure wavelengths in the range from $\lambda_{min} \approx 17$ to $\lambda_{max} \approx 61$ with a fastest growing mode for $\lambda_0 \approx 31.5$. The observed diffusivities and rate constants from all simulations are summarized in Table I of the Appendix.

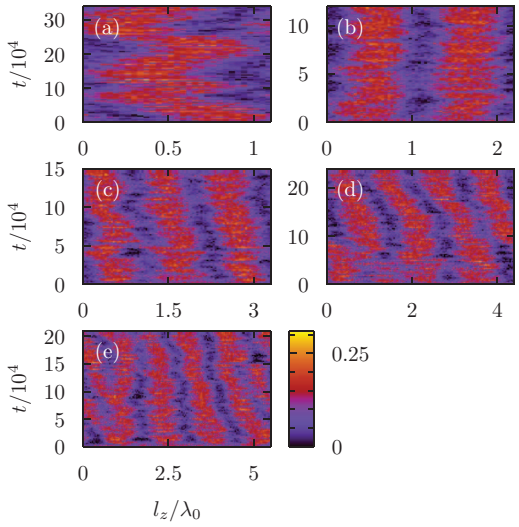

FIG. 2. Space-time plots showing evolution of concentration A (color gradation) along axis z for WCA potential and parameters that give $\lambda_0 \approx 31.5$. Figures 2(a)–2(e) show results of simulations for progressively longer systems.

After estimating the expected wavelength of the structure, we performed simulations for different values of n_z that give system lengths that are close to the multiples of the fastest growing mode: $n_z = 31, 62, 93, 124, 155$, meaning: $\frac{l_z}{\lambda_0} \approx 1.1, 2.2, 3.3, 4.4, 5.5$. Figure 2 presents space-time plots depicting the evolution of concentration of A for these cases.

Clearly, a spatial structure with well defined wavelength, which can be read from the space-time plots, forms in the system. Wavelength of the structure does not depend on system size and is close to the analytical prediction. In some cases fluctuations cause the structure to shift along the z axis. Since the structure is formed from a focus, there are temporal oscillations of concentration of A. We observe that in the larger systems (d) and (e), the time it takes for the fastest growing mode to emerge can be quite long and, before that, transient structures of different wavelengths are seen. In addition, transitions between different wavelengths can happen even later as seen in the case (e). Initially, mode with spatial wavelength $\lambda = 43.6$ dominates, but soon, around $t = 5 \times 10^4$, there is a transition to $\lambda = 34.9$. Later, at $t \approx 11 \times 10^4$, there is another transition to the mode $\lambda = 29.1$, which then returns to the previous mode with larger wavelength at $t \approx 15 \times 10^4$. Transitions between these two modes would probably continue, because they both have very similar eigenvalues. Probability of these transitions could be reduced in a system with larger λ_0, that would contain more particles and where fluctuations would not be significant.

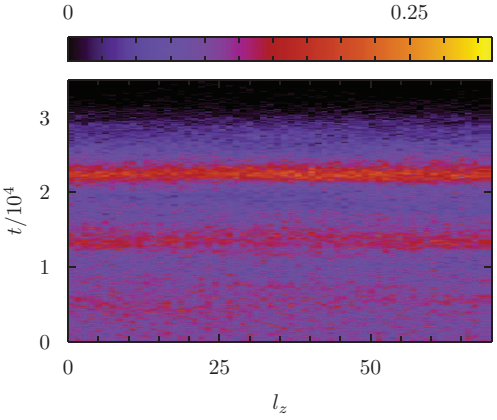

FIG. 3. Same as Fig. 2(b), but for $D_B/D_A \approx 1.5$, i.e., below Turing bifurcation.

Next, we run some reference simulations under similar conditions, but parameters that are not in the Turing region, i.e., in a case when structure should not develop. The idea is to decrease the ratio of diffusivities below the Turing condition. We do it in two different ways. One is to reduce the mass of H particles to $m_H = 1$, which has almost no effect on the trimolecular reaction rate, but change the ratio of diffusion coefficients to $D_B/D_A \approx 1.5$. Because the reaction dynamics is not changed, the initial stationary state is again an unstable focus and we observe oscillatory transition to the state (A_0, B_0), as expected. This dynamics is shown in Fig. 3. The other way of imposing similar diffusivities is to keep $m_H = 10^4$, but remove formation of A-H bonds. Then, the effective trimolecular rate constant is $k_2 \approx 0.15$ and the ratio of diffusivities $D_B/D_A \approx 1$. Since we do not change the unimolecular rate constants, the stationary state is now a stable focus ($A_+ \approx 0.114$, $B_+ \approx 0.066$). In simulations, the system reaches this state and remains homogeneous.

To rigorously check which modes are excited and quantitatively compare stabilities of structures from different simulations, we perform Fourier analysis of the concentration of A along z axis. Positions of particles in the directions x and y are disregarded, since the system remains homogeneous in these directions as l_x and l_y are smaller than λ_{min}. Because, as seen on the space-time plots, the structure can shift along the z axis, we calculate discrete Fourier transforms separately for instantaneous concentration histograms at short time intervals $10^4 \Delta t$. The final Fourier spectrum is obtained by averaging these intermediate transforms. Figure 4 shows the spectra of the simulations discussed so far.

For all the simulations in the Turing region, the spectrum has a maximum in the expected wavenumber range. For the three shorter systems studied, there is a single strongly excited mode. In the longer systems, more modes are allowed by boundary conditions and differences between their eigenvalues are smaller. In that case we observe that more than one mode is excited. This is in agreement with our observations from the space-time plots, that initially a transient structure is formed, which has a longer wavelength than λ_0. For parameters outside of the Turing region the spectrum does not have any maximum above the noise level of thermal fluctuations. We observe that in all cases, except the one without any reactions, the mode with smallest non-zero wavenumber is slightly excited.

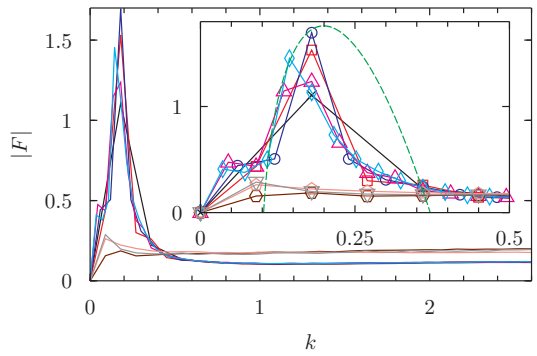

FIG. 4. Complex modulus $|F|$ of discrete Fourier transform versus wave number $k = 2\pi/\lambda$ for WCA potential. Spectra of the results from Fig. 2 are: (a) black, (b) red, (c) dark blue, (d) pink, (e) light blue. For reference we also show spectra of cases when Turing pattern does not develop: without reactions (bronze), without A-H bonds (salmon) and for $m_H = 1$ (grey). The spectra are scaled to obtain $\sum|F_i| = l_z/2\pi$. Average concentration was subtracted from the profile before Fourier analysis in order to obtain $|F_0| = 0$. The spectra are calculated over the time interval $[1, 12] \times 10^4$. The inset shows part of the spectrum around the maxima. The green dashed line is the scaled dispersion relation $\mathrm{Re}(\omega(k)) \times 350$, where $\omega(k)$ is the eigenvalue of mode k predicted by the macroscopic theory.

Next, to test how intermolecular attraction affects structure formation, we run simulations using the LJ potential instead of WCA. The parameter that is affected the most is the trimolecular reaction rate, for $r_r = 0.56$ we got $k_2 \approx 2.1 \times 10^{-2}$. The diffusivities are smaller than in WCA simulations: $D_A \approx 6.9 \times 10^{-3}$ and $D_B \approx 7.2 \times 10^{-2}$. For these values the possible wavelengths are in the range from $\lambda_{min} \approx 30$ to $\lambda_{max} \approx 111$ with a fastest growing mode for $\lambda_0 \approx 56.1$. Again, we performed simulations for different system lengths $\frac{l_z}{\lambda_0} \approx 1, 2, 3, 4$, i.e., for $n_z = 50, 100, 150, 200$. The space-time plots are shown in Fig. 5.

The structure is not as well defined as in WCA simulations and as shown in the space-time plots, it is hard to determine the dominating mode, especially in longer systems. Still, it can be seen that the structure shifts along z axis and that there are temporal oscillations of concentrations, like in WCA simulations. The Fourier spectra of results of LJ simulations are shown in Fig. 6.

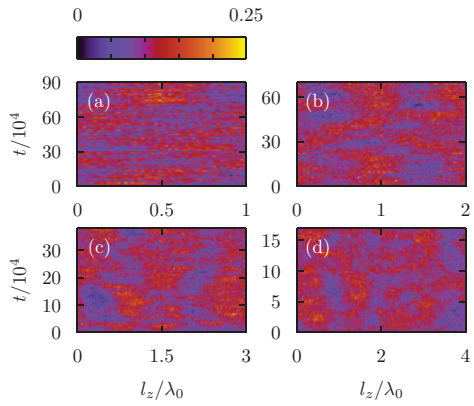

FIG. 5. Same as Fig. 2, but for LJ potential and $\lambda_0 \approx 56.1$.

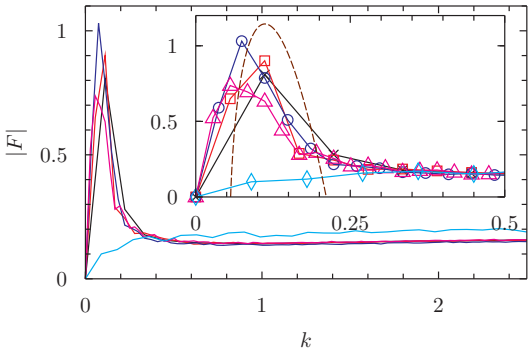

FIG. 6. Same as Fig. 4, but for simulations with LJ potential presented in Fig. 5: (a) black, (b) red, (c) dark blue, and (d) pink. The light blue line is for LJ potential, but without chemical reactions. The brown dashed line in the inset is the scaled dispersion relation $\mathrm{Re}(\omega(k)) \times 8000$. The spectra are calculated over the time interval $[1, 16] \times 10^4$.

Like in the WCA case, the spectra have maxima in the low wavenumber range, which are not seen in simulations without reactions. These maxima have lower values than in WCA simulations and, as seen in the inset, there is a broader range of excited modes. The tendency is that modes with longer wavelengths than predicted by dispersion relation are excited. This may be caused by relatively lower stability of shorter wavelength structures outside the linear regime.

Next, we tested how stability of the structures is affected by the wavelength and see how short a stable structure can be. When decreasing the wavelength we are limited by the size of the system in directions perpendicular to the z axis, because the minimal structure wavelength has to be larger than l_x and l_y in order to get a one-dimensional structure. Therefore, we run a simulation for the WCA potential using same conditions as in Fig. 2, but for $n_z = 17$. Hence, the system length is close to the minimal allowed wavelength and we expect a single wavelength structure. Fig. 7 shows a space-time plot of the result.

The predicted structure develops similarly to the case with longer system size, but around $t \approx 8.5 \times 10^4$ there is a transition to the homogeneous state (A_0, B_0). Probability of such fluctuations-induced transition depends on the total number of particles in the system, so it should be possible to obtain stable structures with wavelength of this order, but in

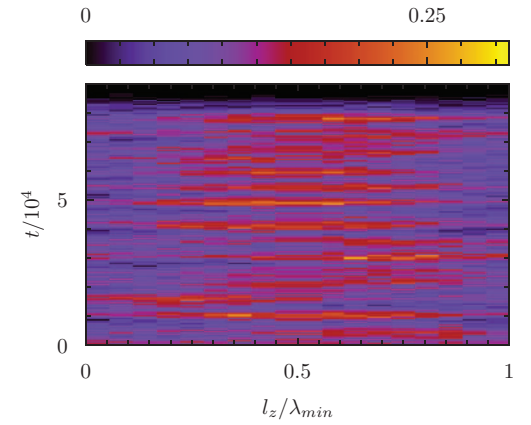

FIG. 7. Same as Fig. 2, but for short system length, close to λ_{min}.

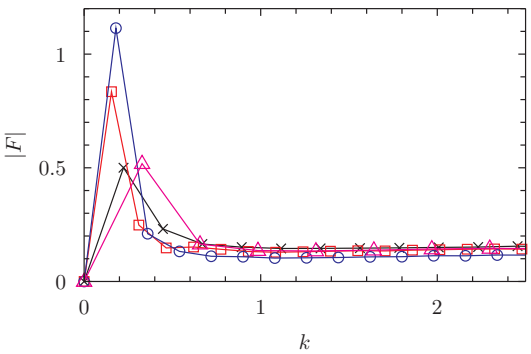

FIG. 8. Comparison of Fourier spectra for different λ_0 and different intermolecular potentials. The blue line is for WCA potential and $\lambda_0 \approx 31.5$, the pink for WCA and $\lambda_{min} \approx 18$ (case from Fig. 7), the red for LJ potential and $\lambda_0 \approx 40$ and the black for LJ and $\lambda_0 \approx 28$. The spectra were calculated the same way as in Fig. 4, but over the time interval $[1, 8.5] \times 10^4$. System length in each case fitted only one wavelength.

larger systems fitting more wavelengths. We do not simulate this case due to long computation times and since it would generate a three-dimensional structure.

To test the stability of the structures of different wavelengths, we ran simulations using the LJ potential for two sets of parameters that give $\lambda_0 \approx 28$ and $\lambda_0 \approx 40$, each time with system length equal to λ_0. The Fourier spectra for different wavelengths are compared in Fig. 8.

It is seen that the maxima are higher for longer wavelengths. This is because for short-scaled structures fluctuations have stronger effect and they broaden and decrease the spectrum around its maximum. Similarly, the maxima are better defined when using WCA potential instead of LJ potential. To directly determine the effect of intermolecular potentials on structure stability, we compare spectra obtained from LJ and WCA simulations done with equal rate constants, i.e., for same dispersion relations. As stated before, LJ simulations for $r_r = 0.56$ result in effective trimolecular rate constant $k_2 \approx 2.1 \times 10^{-2}$. When using WCA potential, we obtain approximately the same value for $r_r = 0.55$. We choose to compare a case of $l_z \approx 3\lambda_0$. Evolution of A concentration is shown in Figs. 5(c) and 9 for LJ and WCA simulations, respectively.

A two-period structure emerges and is stable in WCA simulations, instead of a three-period one predicted by the theoretical analysis. In previous WCA simulations with

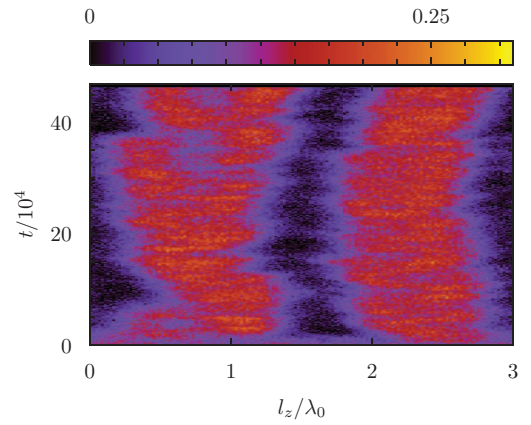

FIG. 9. Same as Fig. 2(c), but for parameters that give $\lambda_0 \approx 56$.

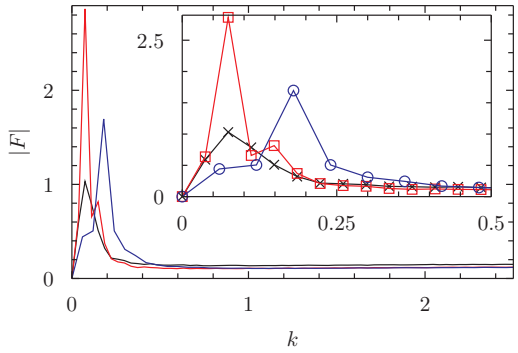

FIG. 10. Comparison of Fourier spectra for different λ_0 and different intermolecular potentials. The black line is for LJ potential with $\lambda_0 \approx 56$, the red is for the same λ_0, but for WCA potential, and the blue line is for WCA potential and $\lambda_0 \approx 31.5$. The spectra were calculated the same way as in Fig. 4, but over the time interval $[1, 14] \times 10^4$. System length in each case fitted three wavelengths.

$\lambda_0 \approx 31.5$ we observed that initially a mode with longer wavelength emerges and later, there is a transition to the expected mode with the highest eigenvalue. We suspect that for $\lambda_0 \approx 56$ such initial structure with $\lambda > \lambda_0$ may dominate the system for a long time, because the internal fluctuations are smaller than for shorter wavelengths. Fourier spectra from these simulations are presented in Fig. 10. For comparison, spectrum for a WCA run with $\lambda_0 \approx 31.5$ and a three-period structure is also plotted.

These spectra confirm that the structure is more stable if the intermolecular attraction is not included and that structures with longer wavelengths are more stable.

So far we have been analysing spatial structures of concentration of one of the reactive species, A. Yet the Turing structure of A and B species also imposes spatial inhomogeneities in concentrations of other species, including species H that are not part of the Gray–Scott reactions scheme. This observation could have important practical consequences. In an experiment, using a single pair of A and B chemicals, one could produce structures of many different molecules playing the role of H. The condition is that these molecules diffuse more slowly and are functionalised to bind A molecules.

V. CONCLUSIONS

Using molecular dynamics simulations we showed that Turing patterns of characteristic length of nanometers can form in bulk chemical reactions, despite strong fluctuations. We obtained structures that have as little as 17 particles/wavelength, but as the wavelength decreases, the pattern becomes less stable. We find that patterns are better defined when using WCA instead of LJ potential, which means that intermolecular attraction has a tendency to prevent formation of structures. Therefore, formation of nanoscale Turing patterns in real systems is more probable in higher temperatures, where repulsive forces become more important.

The formation of Turing patterns requires a specific type of reactions between A and B. Therefore, this mechanism may not seem a robust method for pattern formation at the nanoscale. However, as presented here, the A and B reactions also induce a pattern in the concentration of H molecules, which are not part of the Gray–Scott reactions scheme. Therefore, having a single pair of reactants that can form a Turing pattern, patterns of any large heavy molecules can be obtained if only those molecules are functionalised to bind A molecules.

We observed that initially a structure with longer wavelength than expected from linear stability analysis develops, but after some time there can be a fluctuation-induced transition to the expected mode. Probability of this transition decreases with system size, because fluctuations in larger domains are smaller. Moreover, fluctuations can cause a random shift of the structure in space in the course of time.

The results of this study clearly indicate that the Turing mechanism could be used to produce nanoscale patterns of chemical concentrations.

ACKNOWLEDGMENTS

The work was realized within the International Ph.D. Projects Program co-financed by the Foundation for Polish Science and the European Regional Development Fund within the Innovative Economy Operational Program"Grants for Innovation." P.D. acknowledges the French government fellowship and J.S.H. acknowledges the Lundbeck Foundation for financial support, Grant No. R49-A5634.

APPENDIX: MEASURED MACROSCOPIC CONSTANTS FOR DIFFERENT MICROSCOPIC PARAMETERS

TABLE I. The observed diffusivities of species A and B and observed rate constant k_2 of the trimolecular reaction for different parameters used. The diffusivities were calculated from the mean square displacement of molecules in a homogeneous system in the state (A_+, B_+) without chemical reactions. The rate constant was also calculated for a homogeneous system in this state. Rate constants of other reactions follow from Eqs. (8)–(10). The allowed modes and the fastest growing mode were calculated by linear stability analysis. The cases are ordered as they appear in the text.

Potential	r_r	m_H	k_2	D_A	D_B	λ range	λ_0
WCA	0.56	10^4	7.2×10^{-2}	7.6×10^{-3}	7.5×10^{-2}	(17, 61)	31.5
WCA	0.56	1	7.1×10^{-2}	3.5×10^{-1}	5.3×10^{-1}	None	...
WCA	0.56	10^4 no bonds	1.5×10^{-1}	8.4×10^{-2}	8.4×10^{-2}	None	...
LJ	0.56	10^4	2.1×10^{-2}	6.9×10^{-3}	7.2×10^{-2}	(30, 111)	56.1
LJ	0.575	10^4	8.7×10^{-2}	6.9×10^{-3}	7.2×10^{-2}	(18, 51)	28
LJ	0.566	10^4	3.6×10^{-2}	6.9×10^{-3}	7.2×10^{-2}	(25, 89)	40
WCA	0.55	10^4	1.9×10^{-2}	7.6×10^{-3}	7.5×10^{-2}	(34, 121)	60

[1]A. M. Turing, Philos. Trans. R. Soc., B **237**, 37 (1952).
[2]J. D. Murray, *Mathematical Biology: An Introduction* (Springer, New York, 2002).
[3]V. Castets, E. Dulos, J. Boissonade, and P. de Kepper, Phys. Rev. Lett. **64**, 2953–2956 (1990).
[4]N. Ernst, G. Bozdech, V. Gorodetskii, H.-J. Kreuzer, R. L. C. Wang, and J. H. Block, Surf. Sci. **318**, 1211–1218 (1994).
[5]V. Gorodetskii, J. Lauterbach, H.-H. Rotermund, J. H. Block, and G. Ertl, Nature (London) **370**, 276 (1994).
[6]C. Sachs, M. Hildebrand, S. Völkening, J. Wintterlin, and G. Ertl, Science **293**, 1635 (2001).
[7]T. V. de Bocarmé and N. Kruse, Chaos **12**, 118 (2002).
[8]Y. de Decker and A. S. Mikhailov, Prog. Theor. Phys., Suppl. **165**, 119 (2006).
[9]P. Gaspard, in Proceedings of the International Conference Engineering of Chemical Complexity, Berlin Center for Studies of Complex Chemical Systems, 4–8 July 2011.
[10]B. A. Grzybowski, K. J. M. Bishop, Ch. J. Campbell, M. Fialkowski, and S. K. Smoukov, Soft Matter **1**, 114–128 (2005).
[11]A. Lemarchand and B. Nowakowski, Europhys. Lett. **94**, 48004 (2011).
[12]P. Dziekan, A. Lemarchand, and B. Nowakowski, J. Chem. Phys. **137**, 074107 (2012).
[13]P. Gray and S. K. Scott, J. Phys. Chem. **89**, 22 (1985).
[14]K. Asakura, R. Konishi, T. Nakatani, T. Nakano, and M. Kamata, J. Phys. Chem. B **115**, 3959–3963 (2011).
[15]J. E. Lennard-Jones, Proc. R. Soc. London, Ser. A **106**, 463–477 (1924).
[16]J. D. Weeks, D. Chandler, and H. C. Andersen, J. Chem. Phys. **54**, 5237 (1971).
[17]D. Frenkel and B. Smit, *Understanding Molecular Simulation* (Elsevier, 2001).
[18]See https://code.google.com/p/seplib/ for documentation and source code of the library used for molecular dynamics simulations.